COMMUNICATION

Check for updates

In situ growth and field emission of single-crystal HfC nanotips

Chaojie Li,[ab] Jianxun Xu, ⓘ *[b] Lihua Wang ⓘ *[a] and Xiaodong Han ⓘ [ac]

Nanotips exhibit a low turn-on field and high emission current density, and are considered promising candidates in future cold-field emitters. However, it is difficult to fabricate an emitter with ultra-fine curvature radius, outstanding collimation and stable interfacial adhesion. In this study, we developed an *in situ* technique that enables the fabrication of single-crystal hafnium carbide (HfC) nanotips on top of tungsten (W). The single-crystal feature and outstanding collimation of HfC nanotips were confirmed using transmission electron microscopy (TEM). *In situ* TEM investigation revealed that the HfC nanotip exhibited a typical field-emission turn-on voltage of 128 V (20 nA), and a significant current of $\sim$230 nA at a low extraction voltage of 149 V, when the distance between the tip and extractor is $\sim$50 nm. The field enhancement factor of the HfC nanotip was as high as $\sim 2 \times 10^7$ m^{-1}. These exceptional properties can be attributed to the single-crystal feature, the nanometer-sized apex, the outstanding collimation and the stable interfacial adhesion of the HfC nanotip.

New concepts

This work reports a novel process for fabricating single-crystal nanotips. By combining a micromanipulation system with a pulsed-current quenching process, single-crystal hafnium carbide (HfC) nanotips are obtained through *in situ* growth on the tungsten (W) tip apex. Nanotips, which exhibit low turn-on field and high emission current density due to their high field enhancement factor, are considered promising candidates for future cold-field emitters. However, it is a challenge to fabricate emitters with an ultra-fine curvature radius, outstanding collimation, and stable interfacial adhesion. Using this method, the interface between the fabricated HfC nanotips and the W substrate is more stable than that of emitters fabricated through mechanical transfer. Furthermore, this method ensures that the fabricated HfC exhibits outstanding collimation and a high field enhancement factor of $\sim 2 \times 10^7$ m^{-1} (higher than that of commercial cold-field emission electron sources ($\sim 10^6$)). Benefiting from these properties, the single-crystal HfC nanotips exhibit a low turn-on voltage (128 V/20 nA), a high field emission current ($\sim$230 nA/149 V/50 nm) and stable emission performance. This work provides a novel and facile method for fabricating single-crystal field-emission nano-emitters with stable interfacial adhesion, outstanding apex collimation and a high field enhancement factor.

1. Introduction

A cold-field emitter is widely used in electron microscopes and is a crucial part in determining the resolution and stable performance of modern advanced electron microscopes. The low turn-on field and high emission current density of an emitter are important parameters for characterizing field-emission performance. According to Fowler–Nordheim (FN) theory, the larger the field enhancement factor, the higher the emission electron current density. Previous theoretical and experimental studies have shown that an emitter with a smaller apex curvature usually exhibits a higher field enhancement factor. Therefore, nanostructured emitters with smaller apex curvatures are considered promising candidates for future advanced cold-field emitters. In past decades, many experiments have demonstrated that nanostructures, such as nanotips,[1,2] nanowires,[3] nanotubes,[4,5] nanoparticles[6] and 2D materials,[7] always exhibit a large emission current density, and show potential as next-generation cold-field emission (CFE) electron sources. For instance, many nano-sized emitters can produce a high emission current density, an order of magnitude higher than those of commercial single-crystal W cathode tips.[8]

Thus, in the past few decades, numerous studies have been conducted to fabricate nanostructured emitters. De Jonge *et al.*[9,10] used a piezo-driven micromanipulator to mount nanomaterials onto a W tip. However, this method suffered from low controllability, which compromised the precision of the apical structure and collimation of the nanomaterials. Furthermore, the interfacial adhesion between the nanomaterials and the W

[a] College of Materials Science and Engineering, Beijing University of Technology, Beijing 100124, China

[b] CAS Key Laboratory for Biomedical Effects of Nanomaterials and Nanosafety, CAS Center for Excellence in Nanoscience, National Center for Nanoscience and Technology, Beijing 100190, China

[c] Department of Materials Science and Engineering, Southern University of Science and Technology, Shenzhen 518055, China

substrate was weak,[11] which would significantly affect the stability of the emitter. Di Bartolomeo *et al.* employed carbonaceous deposits induced by electron irradiation to enhance the electrical quality and mechanical stability of the contacts.[12] This method is suitable for larger samples, but usually introduces carbon contamination into small samples. Additionally, many studies have utilized focused ion beam (FIB) techniques to transfer nanomaterials onto W filaments, followed by the deposition of platinum to create nano-emitters.[13,14] The FIB techniques inevitably introduce impurities or undesirable defects in the emitters, leading to degraded emission properties. Nanotips, which were directly grown at the apex rather than being physically assembled, were believed to obtain better interfacial adhesion. This method enabled control over both the collimation and the connection between the nanotips and the substrate,[15,16] while the curvature radius of the emitter was always very large due to the high growth temperature. HfC is a promising field-emission material due to its excellent thermal properties, electrical conductivity, and chemical stability. It is more resistant to ion bombardment than metal, which enhances the longevity and emission stability of the field emitter. Previous reports have demonstrated that nanostructured HfC exhibits outstanding field-emission stability.[17–20] However, most previous methods faced challenges in ensuring both collimation and a stable connection between the nanotips and the substrate. Therefore, there is an urgent need to develop a method that can fabricate single-crystal HfC nanotips with stable interfacial adhesion, excellent collimation and an ultra-fine curvature radius.

In this study, we developed an *in situ* growth method using a micromanipulation system and pulsed-current quenching process, which successfully synthesized a single-crystal HfC nanotip directly on the apex of a W tip. The single-crystal HfC nanotip grew along the [100] direction, with a curvature radius of ∼10 nm. *In situ* field-emission measurement in a TEM revealed that the HfC nanotip exhibited an ultra-low turn-on voltage of 128 V and a high emission current of ∼230 nA (tip–extractor distance of 50 nm). Most importantly, this nanotip demonstrated excellent repeatability and stability during cycle tests across varying transmitting distances. These results provide a simple and rapid method for preparing nanotips applied to CEF electron sources.

2. Experimental section

2.1. Sample preparation

First, the W tip was prepared using electrochemical etching.[21] HfC (99.5%, Zhongnuo Advanced Material Technology Co., Ltd) layers were deposited onto the W substrates using a magnetron sputtering coating system (Lab-18) produced by Lesker in the United States. The HfC thin films on the W substrates were subsequently transferred to the W tip using a micromanipulator (MM3A, Kleindiek Nanotechnic) within a scanning electron microscope (SEM) chamber. Finally, a 100 mA and 1.5 ms pulse current (B2962A series, Keysight) was applied to the HfC/W sample to obtain the HfC nanotip. A schematic of the preparation process of the HfC nanotip is shown in Fig. 1a. W nanotips were also prepared using this method, for comparison (Fig. S1).

2.2. Structural characterization

Characterization of the morphology and structure of the nanotips were carried out using SEM (FEI Quanta 200 FEG), TEM and high-resolution TEM (HRTEM) (FEI Tecnai G2 F20 U-TWIN) installed with energy dispersive X-ray spectroscopy (EDS). Chemical bonding of the synthetic nanotips was determined using electron energy loss spectroscopy (EELS) on an FEI Titan environmental TEM. X-ray photoelectron spectroscopy (XPS) was performed with an Escalab250Xi system using Al Kα X-rays.

2.3. Field emission measurement

The field-emission properties were measured *in situ* using a TEM (FEI Tecnai G2 F20 U-TWIN) under vacuum conditions of ∼2 × 10^{-5} Pa. A schematic diagram of the device for field-emission measurements is shown in Fig. S2: the nanotip was fixed to the piezoelectric-driven part and electrically grounded, serving as the cathode, and a W ball on the opposite side served as the anode. The distance between the nanotip and W ball was adjusted by moving the nanotip, allowing for the measurement of current–voltage (*I–V*) curves at various distances.

3. Results and discussion

Fig. 1a is a schematic of HfC nanotip preparation, and Fig. 1b–d provide the corresponding SEM images showing the morphology and structural features of the W tip, HfC/W tip, and HfC nanotip, respectively. As shown in Fig. 1d, the HfC nanotip exhibited outstanding collimation, which was further confirmed by the TEM image in Fig. 1e. To further verify the reproducibility of the proposed method, Fig. S3 displays another two examples of the fabricated HfC nanotips, showing that the *in situ* growth method, combining a micromanipulation system and pulsed-current quenching, was efficient and reproducible.

The microstructure and crystal structure of the HfC nanotips were further characterized by HRTEM. Fig. 2a shows the TEM image of the fabricated HfC nanotip. The HfC nanotip, which had a size smaller than 20 nm, exhibited a rounded surface with no theoretical cubic facet. Fig. 2b provides the HRTEM image of the HfC nanotip, revealing a curvature radius of ∼8 nm. Fig. 2c displays the inverse fast Fourier transform (FFT) image corresponding to the blue-framed region in Fig. 2b. The measured interplanar spacings were ∼2.68 Å, which can be well indexed to the ($\bar{1}\bar{1}1$) and ($1\bar{1}1$) planes of the face-centered cubic structure of the HfC [011] axis. The image revealed that the nanotip exhibited a single-crystal feature and was collimated along the [100] direction, corresponding to an emission plane of (200). The mapping and EDS analysis confirmed that the HfC nanotip consisted of Hf, C and W elements, as shown in Fig. 2d. Obviously, the uniform distribution of elements and ordered arrangement of atoms confirmed the successful fabrication of the single-crystal HfC nanotip. More importantly, no obvious interface was observed between the W substrate and the HfC nanotip, indicating that the fabricated HfC nanotip
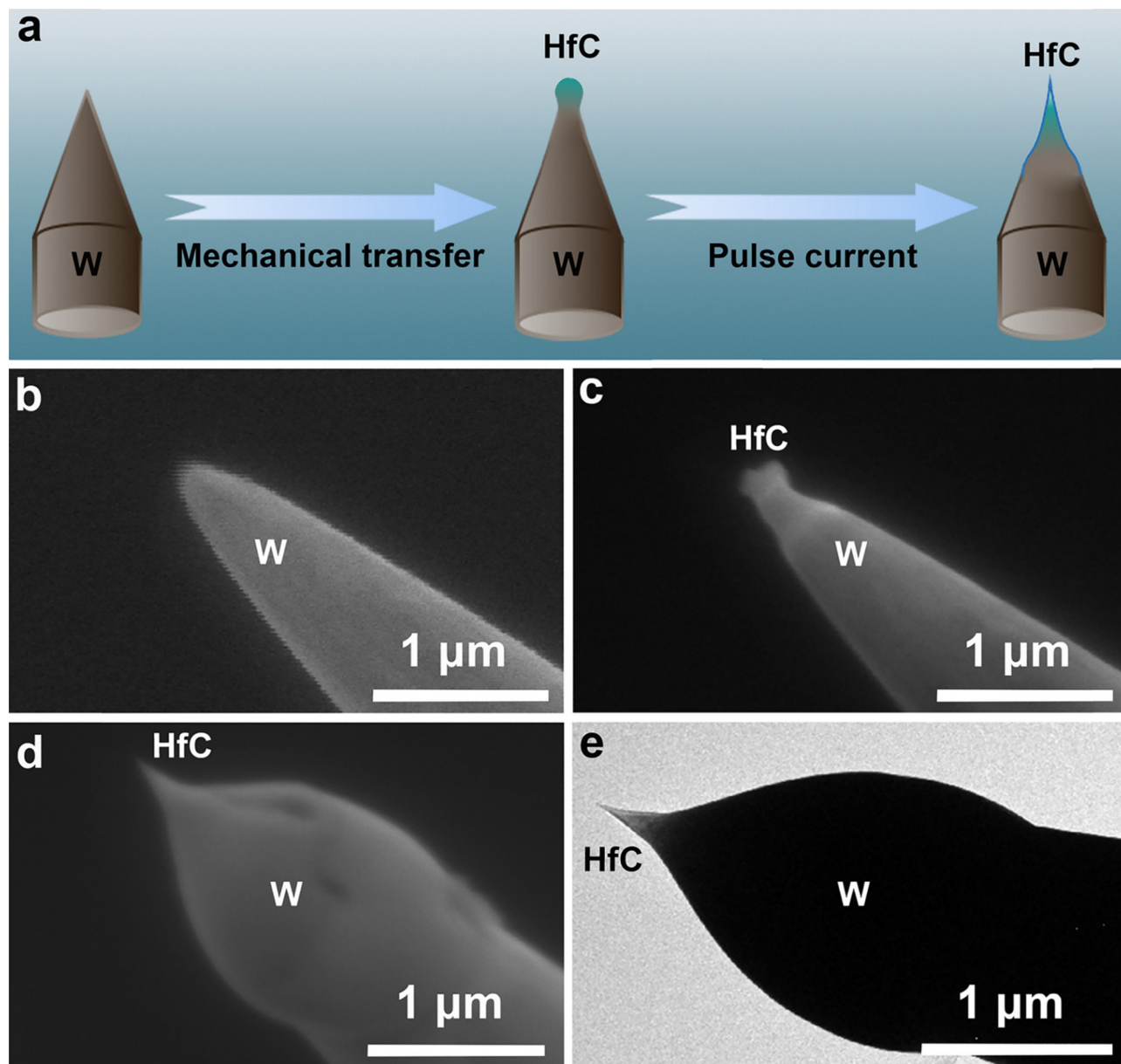
Fig. 1 (a) Schematic illustration of the preparation method for an HfC nanotip; (b)–(d) SEM images of W tip, HfC/W tip, and HfC nanotip, respectively; (e) TEM image of HfC nanotip.

formed a reliable HfC/W connection interface. This was attributed to the fact that the HfC nanotip grew directly at the apex of the W tip. Such a solid connection was essential for the practical application of field-emission nanotips.

To further investigate the chemical composition of the HfC nanotip, EELS and XPS characterizations were performed. As shown in Fig. 3a and b, we have collected the EELS spectra of the HfC nanotip and pure HfC (the corresponding SEM images are provided in Fig. S4). The spectra revealed the presence of C and Hf elements alone, with no detectable oxygen or other impurities, indicating the formation of a pure HfC nanotip. This finding was consistent with the EDS results. As indicated in Fig. 3a, the peaks at 283 eV (1s → Π^*) and 295 eV (1s → σ^*) corresponded to sp^2 and sp^3 hybridized C atoms,

respectively.[22,23] The EELS spectra of Hf were composed of M4, 5 (1700–1900 eV) and M3 (2140 eV) edges (Fig. 3b). Overall, the characteristic C K-edge and Hf M-edge were observed at about 290 and 1800 eV, respectively. A typical XPS survey spectrum of the HfC nanotip, shown in Fig. 3c, exhibits the characteristic peaks of Hf 4f, W 4f, C 1s and O 1s at binding energies of 16.8, 33, 392 and 531.9 eV, respectively. Fig. 3d showed the high-resolution spectra of Hf 4f. Carbide peaks can be identified at 15.5 and 17.2 eV, corresponding to the Hf–C bond, while peaks at 17.8 and 19.2 eV can be assigned to partially oxidized HfC species.[24] Fig. 3e shows the deconvolution diagram of C 1s, where the peak at 283.8 eV can be ascribed to Hf–C for HfC.[25] The C–C, O–C–O and O–C=O peaks located around 284.8, 286.3 and 288.8 eV can be
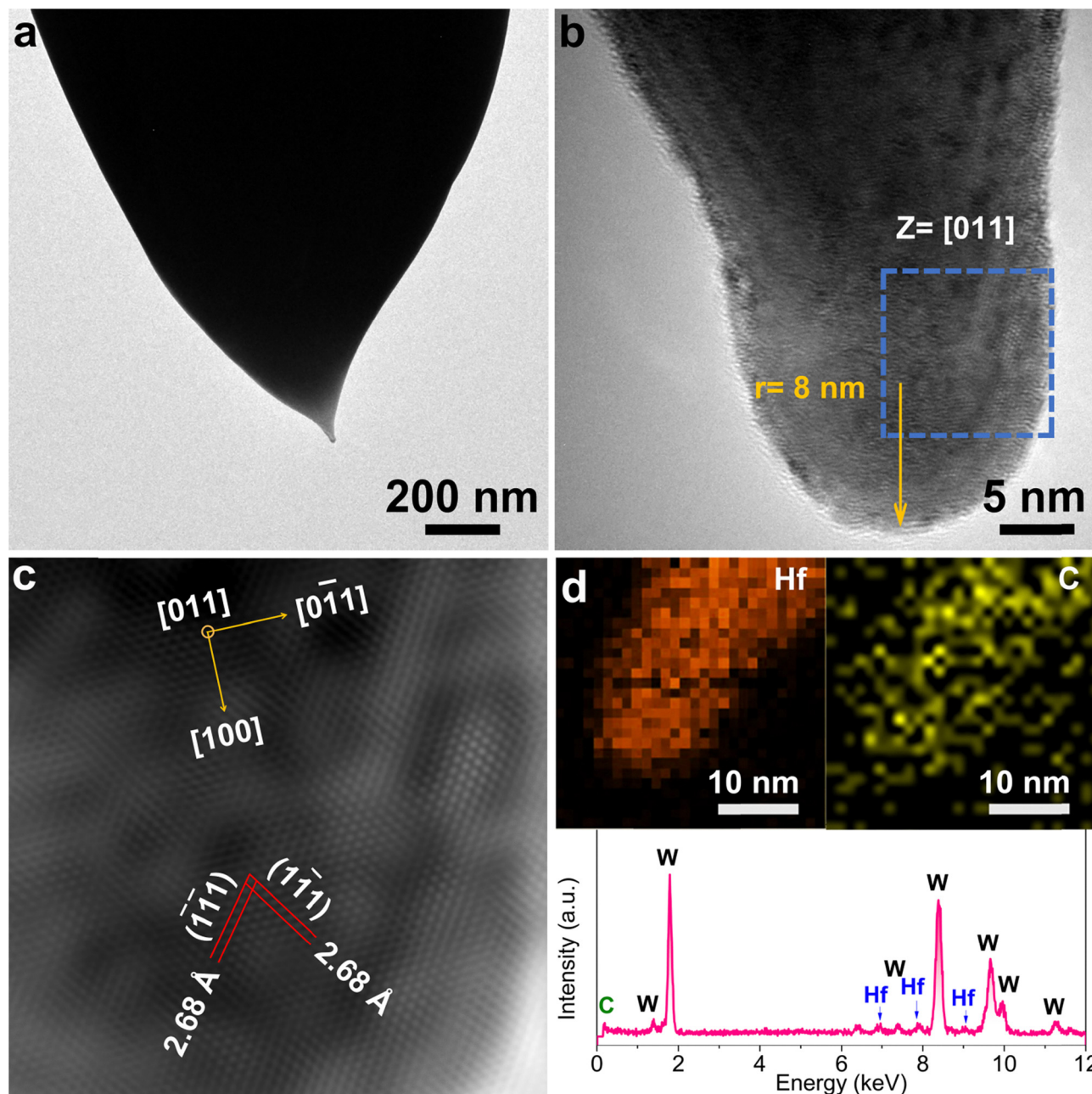
Fig. 2 (a) TEM images of HfC nanotip; (b) HRTEM images of HfC nanotip; (c) inverse FFT crystalline lattice image of HfC nanotip; (d) element distribution maps for Hf and C and EDS analysis of the HfC nanotip.

attributed to the environmental impurities of adventitious carbon in its various states, as reported in the literature.[26–28] Conclusively, the presence of the Hf–C peak directly confirms the successful preparation of the HfC nanotip. Furthermore, the O 1s spectrum shown in Fig. 3f reveals two distinct peaks. Among them, the peak at 530.5 eV is attributed to the binding of Hf–O, the peak at 532.1 eV is related to the hydroxyl substance from water molecules adsorbed on the surface. The appearance of the Hf–O peak may be attributed to the tendency of HfC to oxidize during the transfer or storage processes.[24]

The field-emission properties of the HfC nanotips were investigated using an *in situ* TEM holder. As shown in Fig. 4a,

a W ball was placed at the fixed end and positively biased as the anode, and the nanotip was fixed at the piezo-driven micro-manipulator as the cathode. The distance between the cathode and the anode can be controlled by the movement of the micromanipulator. Fig. 4b shows a typical relationship between the emission current and the extraction voltage (*I–V* curve) from an HfC nanotip with a curvature radius of 8 nm. The emission current of the nanotip increased exponentially with the extrac-tion voltage. Additionally, the *I–V* curves were measured for W with curvature radii of ∼14 nm and ∼150 nm. The W nanotip with a curvature radius of ∼14 nm (the details of its micro-structure are shown in Fig. S5) also showed a similar trend to
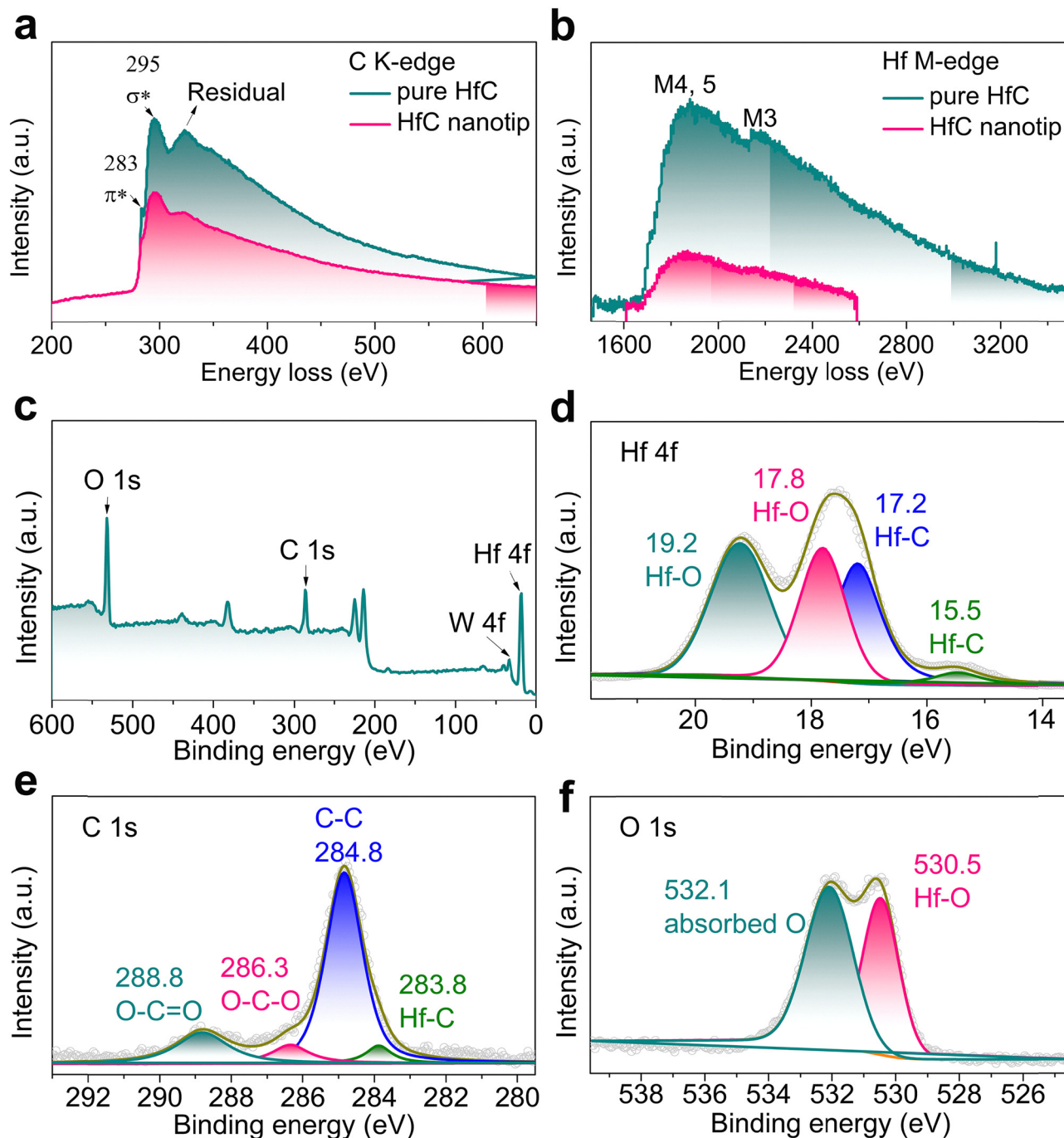
Fig. 3 (a) and (b) EELS analysis of (a) C K-edge and (b) Hf M-edge of pure HfC and HfC nanotip; (c)–(f): (c) survey spectra, (d) Hf 4f, (e) C 1s and (f) O 1s high-resolution XPS spectra of the HfC nanotip.

the HfC nanotip, while the W tip with a curvature radius of ~150 nm showed no emission current. Interestingly, we noticed that the five *I*–*V* cycle curves of the HfC nanotip almost overlap, indicating its emission stability. This stability can be attributed to the better resistance to ion bombardment and gas adsorption of HfC. The field-emission current of the HfC nanotip was as high as 233 nA at an extraction voltage of 149 V, which was apparently higher than that of the W nanotip (126 nA), This difference was mainly due to the larger field

enhancement factor and lower work function of the HfC nanotip.[29] The semi-logarithmic plot of the *I*–*V* curve (in the inset of Fig. 4b) shows that the emission current of the HfC nanotip increased slowly from 80 to 90 V and achieved rapid growth from 90 to 149 V. The emission current of the W nanotip showed no obvious change before 110 V, and the growth rate between 110 V and 149 V was similar to that of the HfC nanotip. While for the W tip, the emission current showed no obvious change from 0 to 149 V.
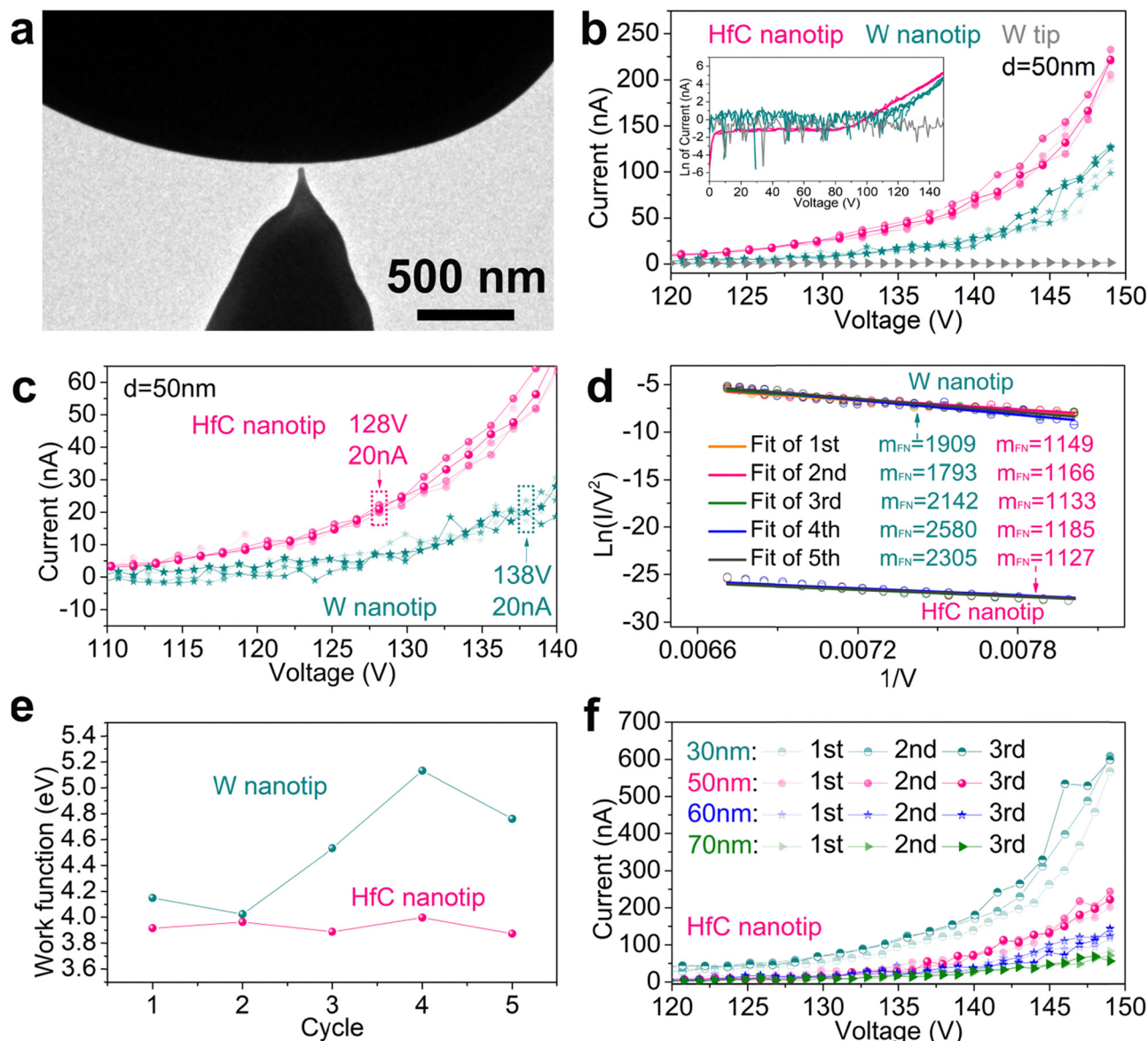
Fig. 4 Measurement of field emission in *in situ* TEM. (a) TEM image showing the W ball and nanotip sample. (b) Field emission *I–V* curves of HfC nanotip, W nanotip and W tip at a tip–W ball distance of 50 nm. The inset in (b) shows a semi-logarithmic plot of (b) over the full voltage range (0–150 V). (c) Local magnification of field emission *I–V* curve shown in (b) and (d) corresponding linearized FN curve. (e) Work functions of the HfC nanotip and W nanotip. (f) Field emission *I–V* curves of the HfC nanotip at various distances.

Fig. 4c provides a magnified image that corresponds to Fig. 4b, clearly showing that the turn-on voltage of the HfC nanotip (defined as the voltage required to generate a 20 nA current) was only $\sim$128 V, while that of the W nanotip was as high as 138 V. Furthermore, we recorded the *I–V* curves of the HfC nanotip at various distances (Fig. 4f), with emission currents of 609 nA, 244 nA, 144 nA, and 83 nA at distances of 30, 50, 60, and 70 nm, respectively. These results demonstrate that the HfC nanotip exhibited both high emission current and stability under a moderately high vacuum. To analyse the turn-on field and field enhancement factor as a function of distance, the FN plots of the HfC nanotip at various distances are plotted in Fig. S6. The field enhancement factor of the HfC nanotip was calculated from substitution of the work function of HfC

(3.929 eV) and the slope of the FN plot (Fig. S6) into eqn (S4). Table S1 lists the turn-on field and corresponding field enhancement factor at various distances (defining the field corresponding to the 20 nA FE current as the turn-on field). The turn-on field decreased and the field enhancement factor increased slightly with increasing tip–extractor distance. The trends in turn-on field and field enhancement factor can be explained by the fact that the distribution of the electric field between tip and extractor changed as the distance increased. When the distance was very small, the tip to extractor approximated a parallel plate configuration, when the field enhancement factor of the HfC nanotip was relatively small. As the HfC nanotip was moved away from the extractor, the parallel plate approximation diminished, and the geometric properties of the
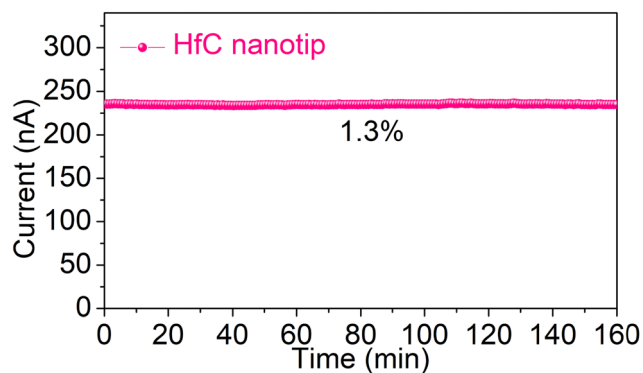
Fig. 5 The FE current–time (I–t) curve of the HfC nanotip.

HfC nanotip exhibited a relatively large enhancement factor, leading to a reduction in turn-on field.[30]

To further explore the emission stability of the HfC nanotip, we measured the FE current–time (I–t) curve under conditions of d = 50 nm and V = 150 V. As shown in Fig. 5, the emission current of the HfC nanotip was stable at 235 nA over 160 min (in a vacuum of 2×10^{-5} Pa), and the emission noise was stable at 1.3%, indicating that the HfC nanotip showed long-term emission stability.

Based on the *in situ* TEM measurements, the work functions of the HfC nanotip can be evaluated. According to FN theory, the slope m_{FN} of the FN equation is given as:[31]

$$\ln\left(\frac{I}{V^2}\right) = \frac{m_{FN}}{V} + b \quad (1)$$

where I is the emission current, V is the extraction voltage, m_{FN} is the slope of the FN plot, and b is the intercept of the FN plot. The FN plots of the HfC nanotip and W nanotip are shown in Fig. 4d. The FN plot had an excellent linear fit with a correlation coefficient above 0.958, indicating that the field emission from the nanotips agreed with a metal-vacuum field-emission model, as described by the FN equation. The slopes m_{FN} of the HfC nanotip were 1149, 1166, 1133, 1185, 1127 eV$^{3/2}$ cm, and of the W nanotip were 1909, 1793, 2142, 2580, 2305 eV$^{3/2}$ cm, respectively.

Then, the work function value can be obtained according to the FN plot (m_{FN}):

$$\Phi = \left[\frac{m_{FN}\beta}{a}\right]^{\frac{2}{3}} = \left[\frac{m_{FN}}{2.96 \times 10^7 \times 5r}\right]^{\frac{2}{3}} = 3.574 \times 10^{-6}\left[\frac{m_{FN}}{r}\right]^{\frac{2}{3}} \quad (2)$$

where Φ is the work function in eV, m_{FN} is the slope of the FN plot, β is the field enhancement factor, $a = 2.96 \times 10^7$, and r is the radius of curvature. For a sharpened emitter with a hemispherical tip of radius r (the unit is cm), β is empirically equal to $1/(5r)$. The field enhancement factor of the HfC nanotip ($\sim 2.5 \times 10^7$ m^{-1}) exceeded that of commercial CFE electron sources ($\sim 10^6$).[32]

The calculated work function values are shown in Fig. 4e. The work functions of the HfC nanotip were 3.917, 3.964, 3.889, 3.999, 3.874 eV, and those of the W nanotip were 4.151, 4.025, 4.532, 5.131, 4.759 eV, respectively. The emission crystal plane

of the HfC nanotip was (200) from Fig. 2b and c. The average work function of HfC (200) was obtained as 3.929 eV, which was slightly lower than that of the HfC (200) nanowire reported in previous studies.[33] The HfC nanotip exhibited a lower work function than the W nanotip, which contributed to the lower turn-on voltage of the HfC nanotip. Table S2 shows the work functions of HfC {100}, and the calculated work functions in this work were close to the literature-reported work functions. We substituted the work function of 3.64 eV and the slope of the FN plot into eqn (S4),[18] and the calculated field enhancement factor of the HfC nanotip was $\sim 1.79 \times 10^7$ m^{-1}. This value was close to the empirical relationship of $\beta = 1/5r = 2.5 \times 10^7$ m^{-1} (r is the radius of curvature with a value of 8 nm). The results reconfirmed that the emission of HfC nanotip in this study was consistent with FN theory. Such a high field enhancement factor also enabled the nanotip-emitters to operate under relatively low applied voltages, making them promising candidates for field emitter applications in moderately high vacuum conditions.

We investigated and compared the cold-field emitters in this work with those reported in the existing literature. As shown in Table S3, the HfC nanotip in this work had a relatively small radius of ~ 8 nm, and a larger field enhancement factor, compared to previously reported emitters. Such a large field enhancement factor allowed the cold-field emitters to operate at a lower turn-on field. As can be seen from Table S3, the HfC nanotip achieved a higher emission current at a lower electric field compared to previous HfC emitters.[8,18] The LaB6 and CeB6 emitters had a low turn-on field due to their extremely low work function and achieved a high emission current at a lower electric field.[34,35] The single multi-walled CNT usually operated with a high emission current ($\sim \mu$A) at a very low electric field, but the emission current typically fluctuated significantly (24%) under continuous emission.[36,37] In our work, the current noise of the HfC nanotip was as low as 1.3% during long-term emission (Fig. 5 I–t curve), suggesting that the HfC nanotip can be considered a promising candidate for future cold-field emitters. Conventionally, three primary methods have been employed to fabricate nano-emitters: mechanical transfer using a micromanipulator in SEM, mechanical transfer using FIB and platinum/carbon deposition, and *in situ* thermal growth. In the first and third methods it was difficult to ensure collimation and a stable connection between the nanotips and the substrate. The second method inevitably introduced impurities or caused structural damage. Our technique provides an alternative route for developing high-performance cold-field emitters.

4. Conclusions

In conclusion, a novel *in situ* growth technique was developed to grow single-crystal HfC nanotips at the apex of a W tip. The HfC nanotip was a single-crystal structure, several nanometers in size, with a [100] crystal orientation and outstanding collimation. *In situ* field-emission tests showed that the single-

crystal HfC nanotips exhibited conventional field-emission behaviour, as described by the FN equation, with a field enhancement factor of up to $\sim 2 \times 10^7$ m^{-1}. Moreover, the HfC nanotips can sustain an emission current up to 609 nA, ascribed to the stability and robustness of HfC. This work provides a novel and facile method for fabricating single-crystal field-emission nano-emitters with stable interfacial adhesion, outstanding apex collimation and a high field enhancement factor.

Conflicts of interest

There are no conflicts to declare.

Data availability

The data that support the findings of this study are available within the article and its SI.

Field emission measurements, SEM images, TEM images and EDS. See DOI: **https://doi.org/10.1039/d5nh00143a**

Acknowledgements

References

1 F. Houdellier, L. Knoope, C. Gatel and A. Mackie, *Ultramicroscope*, 2015, **151**, 107–115.

2 O. Bhorade, B. Deconihout, I. Blum, S. Moldovan, J. Houard, A. Normand, K. Jagtap, M. More and A. Vella, *Nanoscale Adv.*, 2023, **5**(9), 2462–2469.

3 H. Zhang, J. Tang, Q. Zhang, G. Zhao, G. Yang, J. Zhang, O. Zhou and L. C. Qin, *Adv. Mater.*, 2005, **18**(1), 87–91.

4 N. de Jonge, *Adv. Imaging Electron Phys.*, 2009, **156**, 203–233.

5 S. G. Sarkar, S. Acharya, R. Alexander, A. Kaushal, J. Bahadur, J. Mondal and K. Dasgupta, *Chem. Eng. J.*, 2025, **503**, 158622.

6 A. Di Bartolomeo, M. Passacantando, G. Niu, V. Schlykoe, G. Lupina, F. Giubileo and T. Schroeder, *Nanotechnology*, 2016, **27**, 485707.

7 D. Nguyen, S. Suzuki, S. Kato, B. To, C. Hsu, H. Murata, E. Rokuta, N. Tai and M. Yoshimura, *ACS Nano*, 2015, **9**, 3206–3214.

8 S. Tang, J. Tang, T.-W. Chiu, W. Hayami, J. Uzuhashi, T. Ohkubo, F. Uesugi, M. Takeguchi, M. Mitome and L.-C. Qin, *Nano Res.*, 2020, **13**(6), 1620–1626.

9 N. d Jonge, J. T. Oostveen, T. v Rooij and M. Allioux, *Adv. Imaging Electron Phys.*, 2005, **156**, 203–233.

10 N. De Jonge and J. M. Bonard, *Philos. Trans. R. Soc., A*, 2004, **362**(1823), 2239–2266.

11 N. de Jonge, Y. Lamy, K. Schoots and T. H. Oosterkamp, *Nature*, 2002, **420**, 393–461.

12 A. Gillo, M. Pssacantando, A. Zak, A. Pelella and A. Di Bartolomeo, *Small*, 2020, **16**, 2002880.

13 H. Zhang, J. Tang, J. Yuan, Y. Yamauchi, T. T. Suzuki, N. Shinya, K. Nakajima and L.-C. Qin, *Nat. Nanotechnol.*, 2015, **11**(3), 273–279.

14 S. Tang, J. Tang, T.-W. Chiu, J. Uzuhashi, D.-M. Tang, T. Ohkubo, M. Mitome, F. Uesugi, M. Takeguchi and L.-C. Qin, *Nanoscale*, 2020, **12**(32), 16770–16774.

15 P. Yazdanfar, H. Heydarian and B. Rashidian, *Nanophotonics*, 2022, **11**(21), 4671–4686.

16 X. Shao, A. Srinivasan, W. K. Ang and A. Khursheed, *Nat. Commun.*, 2018, **9**(1), 1288.

17 C. Kealhofer, S. M. Foreman, S. Gerlich and M. A. Kasevich, *Phys. Rev. B: Condens. Matter Mater. Phys.*, 2012, **86**, 3.

18 T.-W. Chiu, J. Tang, S. Tang, J. Yuan and L.-C. Qin, *Phys. Status Solidi A*, 2020, **217**(10), 2070036.

19 J. Yuan, H. Zhang, J. Tang, N. Shinya, K. Nakajima, L. C. Qin and R. Riedel, *J. Am. Ceram. Soc.*, 2012, **95**(7), 2352–2356.

20 K. J. Kagarice, G. G. Magera, S. D. Pollard and W. A. Mackie, *J. Vac. Sci. Technol., B*, 2008, **26**(2), 868–871.

21 Y. Ge, L. Xu, X. Lu, J. Xu, J. Liang and Y. Zhao, *Small*, 2018, **14**, 1801288.

22 L. Yang, A. Neville, A. Brown, P. Ransom and A. Morina, *Tribol. Lett.*, 2015, **57**, 2.

23 J. Prías-Barragán, K. Gross, H. Ariza-Calderón and P. Prieto, *Sci. Technol. Outreach J.*, 2018, **1**, 9–47.

24 K. Hans, S. Latha, P. Bera and H. C. Barshilia, *Sol. Energy Mater. Sol. Cells*, 2018, **185**, 1–7.

25 M. Farhan, O. Fayyaz, M. Nawaz, A. B. Radwan and R. A. Shakoor, *Mater. Chem. Phys.*, 2022, **291**, 126696.

26 T. L. Barr and S. Seal, *J. Vac. Sci. Technol., A*, 1995, **13**(3), 1239–1246.

27 D. J. Miller, M. C. Biesinger and N. S. McIntyre, *Surf. Interface Anal.*, 2002, **33**(4), 299–305.

28 H. Piao and N. S. McIntyre, *Surf. Interface Anal.*, 2002, **33**(7), 591–594.

29 J. Yuan, H. Zhang, J. Tang, N. Shinya, K. Nakajima and L.-C. Qin, *Appl. Phys. Lett.*, 2012, **100**(11), 113111.

30 R. C. Smith, D. C. Cox and S. R. P. Silva, *J. Vac. Sci. Technol., B*, 2008, **26**, 842.

31 W. A. Mackie, J. L. Morrissey, C. H. Hinrichs and P. R. Davis, *J. Vac. Sci. Technol., A*, 1992, **10**(4), 2852–2856.

32 A. V. Crewe, D. N. Eggenberger, J. Wall and L. M. Welter, *Rev. Sci. Instrum.*, 1968, **39**(4), 576–583.

33 J. Wang and S.-q Wang, *Appl. Surf. Sci.*, 2015, **357**, 1046–1052.

34 S. Tang, J. Tang, J. Uzuhashi, T. Ohkubo, W. Hayami, J. Yuan, M. Takeguchi, M. Mitome and L. Qin, *Nanoscale Adv.*, 2021, **3**, 2787–2792.

35 S. Tang, J. Tang, Y. Wu, Y. Chen, J. Uzuhashi, T. Ohkuboa and L. Qin, *Nanoscale*, 2021, **13**, 17156–17161.

36 C. Kim, H. Jang, S. Lee, H. Lee, Y. Roh, L. Rhee, E. Lee, H. Yang and D. Kim, *Nanotechnology*, 2006, **17**, 5180–5184.

37 C. Jin, J. Wang, M. Wang, J. Su and L. Peng, *Carbon*, 2005, **43**, 1026–1031.